Journal of Applied Mechanics and Technical Physics, Vol. 42, No. 5, pp. 741–747, 2001

LIFTING OF DUST PARTICLES BEHIND A REFLECTED SHOCK WAVE SLIDING ABOVE A PARTICLE LAYER

S. P. Kiselev and V. P. Kiselev

UDC 532.539

The paper presents results of mathematical simulation of particle lifting behind a shock wave reflected from the face wall and sliding above the particle layer. It is shown that particle lifting occurs in a vortex initiated in the gas when the shock wave is reflected from the wall.

1. Many works deal with the problem of lifting of dust particles behind a sliding shock wave [1–6]. This process plays an important role in the formation of a two-phase gas–particle mixture filling up some space. At present, dust lifting behind a transmitted shock wave has been studied in detail. In this case, the gas follows the shock wave with a high velocity. The kinetic energy of the gas is transformed into the energy of random motion of particles through turbulence mechanisms [4] and the Magnus force [5, 6]. Dust lifting behind a shock wave reflected from the face wall has been less adequately studied. Here, the mean gas velocity behind the reflected shock wave is close to zero, and the particles seemingly cannot lift from the surface. However, we can observe dust lifting behind a reflected shock wave from the experiments [1, 6]. It was assumed [7, 8] that the particles are lifted in a vortex formed behind the reflected shock wave. This assumption is further developed in the present paper.

2. We consider a planar channel whose left side is open, and the right one is closed by a face wall (Fig. 1). Assume that the channel of length L and height H is filled by air with a pressure p^0 at the initial time $t = 0$. We observe a cloud, which is a mixture of air and spherical particles of diameter d, near the channel bottom in a layer of thickness h. The shock wave comes into the channel from the left and propagates with a velocity D. Hereinafter, this shock wave is called a transmitted one. After reflection from the right face wall, a reflected shock wave propagating in the opposite direction arises. Note, a layer of particles was poured in experiments onto the channel bottom or into an embedded cell [1, 5, 6]; therefore, the particles were in a dense packed state. Behind the transmitted shock wave, the particles in the upper layer are accelerated by the gas, collide with the particles from bottom layers, and transmit their kinetic energy to bottom particles. As a result, stability of the dense particle layer is lost; the latter is expanded and becomes rarefied. After that, collisions between the particles become rare and do not play a significant role in particle lifting. The process of stability loss in a dense cloud is not considered in the present work, and the cloud is assumed to be rarefied. This allows us to ignore collisions between the particles, which significantly simplifies the mathematical formulation of the problem.

The motion of particles is described by the collisionless kinetic equation, while the gas flow is described by the equations of a dusty gas. This model is described in detail in [9]; the corresponding equations have the form

$$\frac{\partial f}{\partial t} + v_{2x}\frac{\partial f}{\partial x} + v_{2y}\frac{\partial f}{\partial y} + \frac{\partial a_x f}{\partial v_{2x}} + \frac{\partial a_y f}{\partial v_{2y}} + \frac{\partial q f}{\partial T_2} = 0,$$

$$f = f(t, x, y, v_{2x}, v_{2y}, r, T_2), \qquad n = \int f\, dV, \qquad m_2 = \frac{4\pi}{3}\int r^3 f\, dV,$$

$$dV = dv_{2x}\, dv_{2y}\, dr\, dT_2, \qquad m_1 + m_2 = 1, \qquad q = 2\pi\lambda r \mathrm{Nu}(T_1 - T_2)/(c_s m_p),$$

$$a_x = a'_x - \frac{1}{\rho_{22}}\frac{\partial p}{\partial x}, \qquad a_y = a'_y - \frac{1}{\rho_{22}}\frac{\partial p}{\partial y},$$

Institute of Theoretical and Applied Mechanics, Siberian Division, Russian Academy of Sciences, Novosibirsk 630090. Translated from Prikladnaya Mekhanika i Tekhnicheskaya Fizika, Vol. 42, No. 5, pp. 8–15, September–October, 2001. Original article submitted May 28, 2001.

0021-8944/01/4205-0741 $25.00

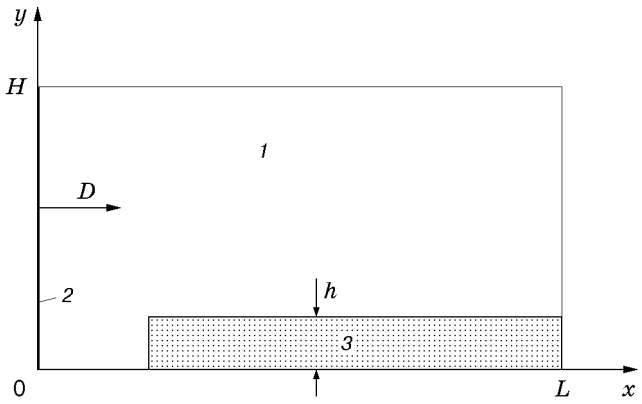

Fig. 1. Diagram of the channel, cloud of particles, and shock wave at the initial time: 1) air; 2) shock wave; 3) mixture of air and particles.

$$a'_x = \frac{v_{1x} - v_{2x}}{\tau} + 2\,\frac{\rho_{11}}{\rho_{22}}(v_{1y} - v_{2y})\omega_z, \qquad a'_y = \frac{v_{1y} - v_{2y}}{\tau} - 2\,\frac{\rho_{11}}{\rho_{22}}(v_{1x} - v_{2x})\omega_z - g,$$

$$\frac{1}{\tau} = \frac{3}{4}\,\frac{\mu \mathrm{Re}}{\rho_{22} d^2}\,C_d(\mathrm{Re}, \mathrm{M}_{12}), \qquad m_p = \frac{4\pi}{3}\,r^3 \rho_{22},$$

$$C_d(\mathrm{Re},\, \mathrm{M}_{12}) = \Big(1 + \exp\Big(-\frac{0.43}{\mathrm{M}_{12}^{4.67}}\Big)\Big)\Big(0.38 + \frac{24}{\mathrm{Re}} + \frac{4}{\sqrt{\mathrm{Re}}}\Big),$$

$$\mathrm{Re} = \rho_{11}|\boldsymbol{v}_1 - \boldsymbol{v}_2| d/\mu, \qquad \mathrm{M}_{12} = |\boldsymbol{v}_1 - \boldsymbol{v}_2|/c, \qquad c = \sqrt{\gamma p/\rho_{11}},$$

$$\mathrm{Nu} = 2 + 0.6\,\mathrm{Re}^{0.5}\mathrm{Pr}^{0.33}, \qquad \mathrm{Pr} = c_p \mu/\lambda, \qquad E_1 = c_v T_1,$$

$$\frac{\partial \varphi}{\partial t} + \frac{\partial F}{\partial x} + \frac{\partial G}{\partial y} + \Phi = 0, \qquad \rho_1 = \rho_{11} m_1, \qquad p = (\gamma - 1)\rho_{11} E_1, \tag{1}$$

$$\varphi = \begin{bmatrix} \rho_1 \\ \rho_1 v_{1x} \\ \rho_1 v_{1y} \\ \rho_1 (E_1 + (v_{1x}^2 + v_{1y}^2)/2) \end{bmatrix}, \qquad F = \begin{bmatrix} \rho_1 v_{1x} \\ \rho_1 v_{1x}^2 + p m_1 \\ \rho_1 v_{1x} v_{1y} \\ \rho_1 v_{1x} A_1 \end{bmatrix},$$

$$G = \begin{bmatrix} \rho_1 v_{1y} \\ \rho_1 v_{1x} v_{1y} \\ \rho_1 v_{1y}^2 + p m_1 \\ \rho_1 v_{1y} A_1 \end{bmatrix}, \qquad \Phi = \begin{bmatrix} 0 \\ \Phi_1 \\ \Phi_2 \\ A_2 \end{bmatrix},$$

$$A_1 = E_1 + p m_1/\rho_1 + (v_{1x}^2 + v_{1y}^2)/2, \qquad \rho_{22} = \mathrm{const},$$

$$A_2 = v_{1x}\Phi_1 + v_{1y}\Phi_2 + p\Big(\frac{\partial m_1}{\partial t} + v_{1x}\,\frac{\partial m_1}{\partial x} + v_{1y}\,\frac{\partial m_1}{\partial y}\Big) - \Phi_3,$$

$$\Phi_1 = -p\,\frac{\partial m_1}{\partial x} + \int m_p a'_x f\, dV, \qquad \Phi_2 = -p\,\frac{\partial m_1}{\partial y} + \int m_p a'_y f\, dV,$$

$$\Phi_3 = \int m_p \Big((v_{1x} - v_{2x})a'_x + (v_{1y} - v_{2y})a'_y - c_s q\Big) f\, dV.$$

Here the subscripts 1 and 2 refer to the gas and particle parameters, respectively; f is the distribution function of particles; v_{1x} and v_{1y} are the gas velocities along the x and y axes, respectively, ρ_{11}, ρ_1, T_1, p, γ, E_1, and m_1 are the true density, mean density, temperature, pressure, ration of specific heat, specific energy, and volume concentration of the gas, respectively; n is the number concentration of particles; v_{2x}, v_{2y} and a_x, a_y are the particle

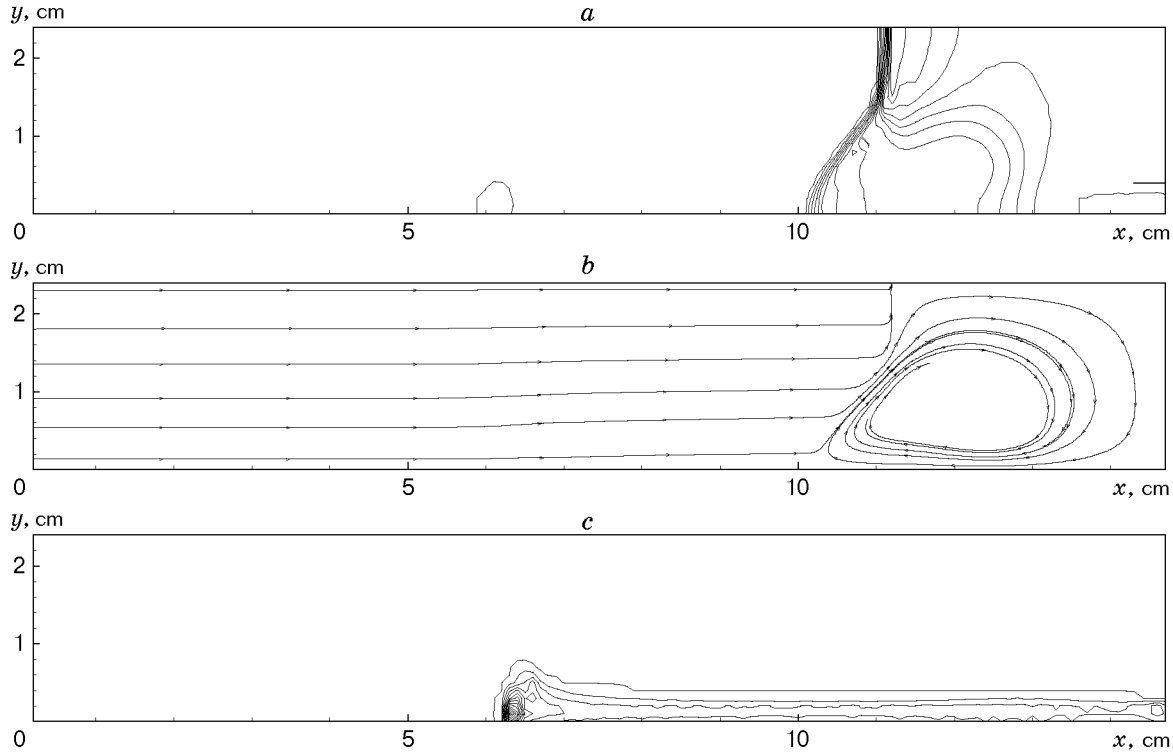

Fig. 2. Gas-particle flow pattern for $t = 240$ μsec: (a) isobars; (b) streamlines; (c) isolines $m_2(x, y) = \text{const}$.

velocities and accelerations along the x and y axes, respectively, ρ_{22}, r, T_2, and m_2 are the true density, radius, temperature, and volume concentration of the particles, respectively; μ, λ, c_v, and c are the viscosity, thermal conductivity, heat capacity at constant volume, and velocity of sound in the gas, respectively; m_p and ω_z are the mass and angular velocity of particles, respectively; g is the acceleration of gravity; Re, Nu, Pr, and M_{12} are the Reynolds, Nusselt, Prandtl, and Mach numbers. Contrary to [9], the force of gravity $m_p\boldsymbol{g}$ and the Magnus force $\boldsymbol{F}_{\mathrm{M}} = \pi d^3\rho_{11}(\boldsymbol{v}_1 - \boldsymbol{v}_2) \times \boldsymbol{\omega}/3$ are added to the equations of motion of the particles and gas in (1) (the last formula was obtained in [10] under the condition $\mathrm{Re}_\omega = d^2\omega/\nu \gg 1$). System (1) is not closed because there is no equation for $\boldsymbol{\omega}$ in the given model. The angular velocity of particle rotation $\boldsymbol{\omega}$ is determined by collisions of particles in the dense layer and is found from the experiment [5, 6].

The boundary conditions for system (1) on the side walls and right end-face wall of the channel are formulated as follows: no-slip conditions for the gas and the condition of specular reflection for the particles. The condition of symmetry is set for the gas equations at the left open end of the channel (Fig. 1). The gas with a pressure p^0 and temperature T_1^0 is in a quiescent state at the time $t = 0$ ahead of the shock wave: $v_{1x}^0 = v_{1y}^0 = 0$. Computations are performed for the following parameters behind the shock wave:

$$v_{1x} = (1 - \xi)c_0(\mathrm{M}_0 - 1/\mathrm{M}_0), \qquad v_{1y} = 0,$$

$$p = p^0((1 + \xi)\mathrm{M}_0 - \xi), \qquad \rho_{11} = \rho_{11}^0\mathrm{M}_0^2/(1 - \xi + \xi\mathrm{M}_0^2),$$

$$\xi = (\gamma - 1)/(\gamma + 1), \qquad \mathrm{M}_0 = D/c_0, \qquad c_0 = \sqrt{\gamma p^0/\rho_{11}^0}.$$

Here M_0 is the Mach number of the shock wave and c_0 is the velocity of sound ahead of the shock wave. At $t = 0$, the particles are in the rectangular layer of height h in a motionless state, the volume concentration of particles is m_2^0, and the temperature is the same as the air temperature. Therefore, the distribution function has the form

$$f^0 = (6m_2^0/(\pi d^3))\delta(r - d/2)\delta(T_2 - T_1^0)\delta(v_{2x})\delta(v_{2y}).$$

System (1) was numerically solved by the method described in [9]. The equations for the gas were approximated on a uniform grid by a third-order finite-difference scheme. The cloud of particles was divided into cells

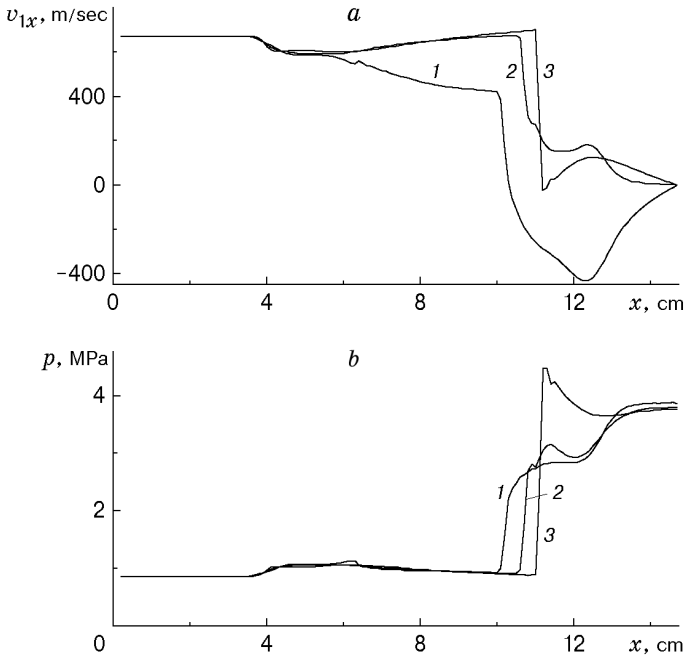

Fig. 3. Gas velocity (a) and pressure (b) distributions along the x axis for $t = 240$ μsec: 1) $y_1 = 0.2$ cm; 2) $y_2 = 1$ cm; 3) $y_3 = 2.2$ cm.

whose equations of motion coincided with the equations of characteristics of the kinetic equation of particles in (1). Because of the absence of collisions, the number of particles remained the same in every cell.

3. A cloud of particles of Plexiglas is located in a channel of rectangular form of length $L = 15$ cm and height $H = 2.4$ cm. The cloud length is 14.7 cm, and its height is $h = 0.25$ cm (Fig. 1). The particle diameter is $d = 200$ μm, the density is $\rho_{22} = 1.2$ g/cm^3, and the volume concentration is $m_2^0 = 10^{-2}$. The cloud of particles is struck by a shock wave (Fig. 1) whose Mach number is $\mathrm{M}_0 = 2.7$, the pressure in air ahead of the shock wave is $p^0 = 10^5$ Pa, the temperature is $T_1^0 = 293$ K, the ratio of specific heats is $\gamma = 1.4$, and the kinematic viscosity of the gas is $\nu = 0.15$ cm^2/sec. These parameters of the particle cloud and shock wave coincide with the experimental parameters of lifting of Plexiglas dust particles behind the transmitted shock wave [5, 6]. An angular velocity of particles ω arises in the case of non-central collisions of particles in the dense layer and is determined by the velocity of random motion of particles v_0 in the dense layer by the formula $\omega_0 = 1.5v_0/d$ [11]. When the stability is lost and the layer is expanded, the collisions between the particles cease, and the frequency of the particle rotation gradually decreases under the effect of viscosity. It was assumed [5, 6] that the value of ω remains constant upon expanding of the layer, and the particles behind the transmitted shock wave are lifted under the effect of the Magnus force. As a result, it was found [5, 6] that $\omega = \omega_0 \approx 6.4 \cdot 10^4$ sec^{-1}, and the velocity of random motion of particles was $v_0 \approx 8$ m/sec. This value of ω_0 was used in system (1) for setting ω_z. Note that the particles start to rotate with an angular velocity ω_0 at some time t' after arrival of the shock wave. The delay t' is determined by the processes of stability loss of the dense layer of particles and evaluated from the experimental data [5, 6]. According to [5, 6], the presence of the weighted particles in the gas stream is registered within 70–80 μsec; therefore, $t' \approx 100$ μsec.

In line with the above reasoning, we assume that $\omega_z = 0$ at $t < t^*$ and $\omega_z \neq 0$ at $t > t^*$, where $t^* = \xi/D + t'$; $\xi = x_p|_{t=0}$ is the coordinate on the x axis at the time $t = 0$. Since rotation of particles results from collisions of randomly moving particles in the dense layer, the vector of angular velocity also has a random orientation. To take this into account in assigning ω_z at the time $t = t^*$ in a given point of space, the particles in a cell are divided into five equal subcells, where ω_z is assumed to be equal to $-\omega_0$, $-\omega_0/2$, 0, $\omega_0/2$, and ω_0. The value of t' is equal to 100 μsec. In estimates, the decay of the angular velocity owing to viscosity $\tau_\omega \approx \rho_{22}/(3\rho_{11}C_d\omega)$ is approximately equal to $3 \cdot 10^4$ μsec for the given conditions ($\omega \approx 10^4$ sec^{-1}, $\mathrm{Re}_\omega \approx 20$, and $C_d \approx 1$). Since the characteristic time of the process is $t \approx 10^3$ μsec, and we can ignore angular velocity variation, the value of ω_z remains constant in each cell at $t > t^*$.

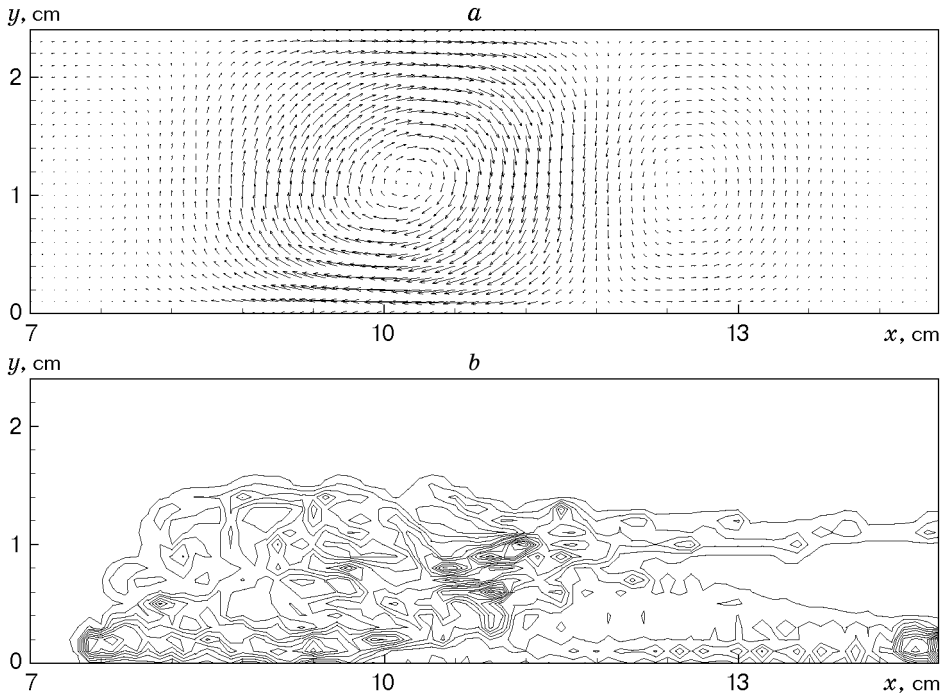

Fig. 4. Gas-particle flow pattern for $t = 560$ μsec: (a) field of velocities $\boldsymbol{v}_1$; (b) isolines $m_2(x, y) = \text{const}$.

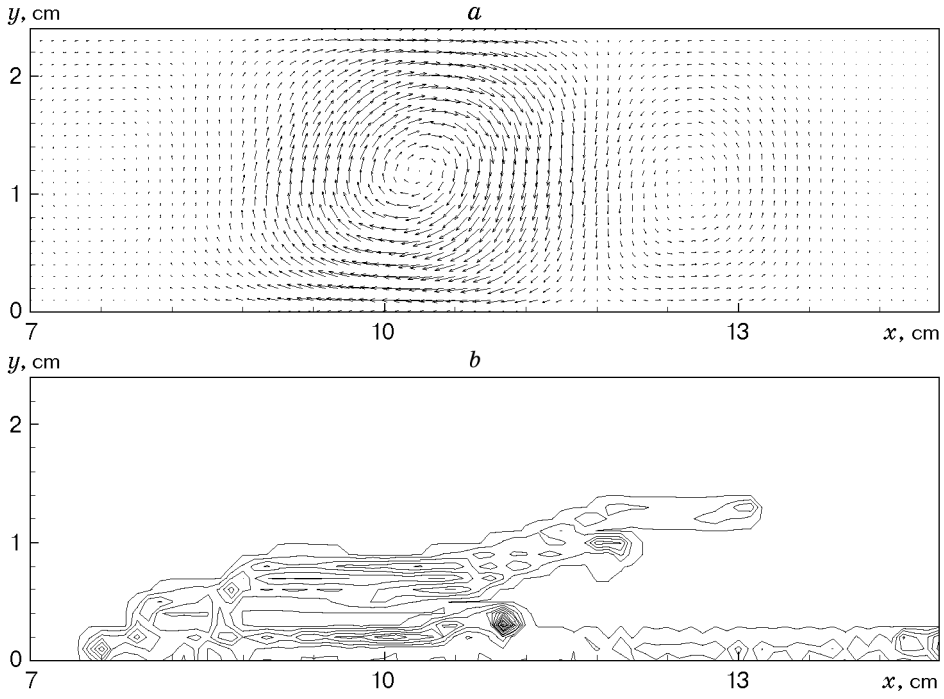

Fig. 5. Gas-particle flow pattern for $t = 560$ μsec, $\boldsymbol{F}_{\mathrm{M}} = 0$: (a) field of velocities $\boldsymbol{v}_1$; (b) isolines $m_2(x, y) = \text{const}$.

The computations show that the normal shock wave transits the channel rather quickly. At the time $t \approx 140$ μsec, it reflects from the right end-face wall of the channel. The cloud was not distorted significantly during this time. Figure 2 shows the flow behind the reflected shock wave at the time $t = 240$ μsec. The reflected shock wave acquires a λ-structure, and a vortex originating behind it plays a significant role in particle lifting. The formation of the λ-structure of the reflected shock wave sliding above the cloud was experimentally observed in [6]. The cloud is not distorted significantly at $t = 240$ μsec, and the particles are drifted to the right towards the face wall (Fig. 2c). As is shown below, the initiation of the vortex flow is caused by the formation of the λ-structure of the reflected shock wave because of nonuniformity of the gas flow behind the transmitted shock wave.

Figure 3a shows the velocity distribution $v_{1x}(x, y)$ in three sections $y = y_i$ parallel to the bottom wall of the channel. The velocity $v_{1x}(x, y)$ is shown near the bottom wall of the channel in the section $y_1 = 0.2$ cm, in the middle of the channel in the section $y_2 = 1$ cm, and near the upper wall in the section $y_3 = 2.2$ cm. The corresponding pressure distributions are plotted in Fig. 3b. Wide fluctuations of velocity and pressure correspond to the front of the reflected shock wave in the sections $y = y_i$. The gas velocity near the bottom wall ahead of the shock wave is smaller than far from it. At the same time, the pressure ahead the reflected shock wave is uniform and independent of the ordinate y. A decrease in v_{1x} near the lower wall results from gas deceleration by the particles of the cloud, and the pressure uniformity is ensured by its equalization by acoustic waves. As a consequence of the nonuniformity of the dependence $v_{1x}(y)$, the reflected shock wave near the bottom wall propagates to the left with a higher velocity than far from it, and its front acquires a typical λ-form in the course of time. Denoting the gas parameters ahead of and behind the reflected shock wave by the subscripts 1 and 2, respectively, we evaluate the pressure behind the reflected shock wave $p_2 \approx \rho_1(v_{1x} - D)^2 + p_1$ using the law of momentum conservation. From the above reasoning, it follows that the difference $v_{1x} - D$ decreases while moving closer to the bottom wall, which leads to the corresponding decrease in pressure p_2. This conclusion correlates with calculation results (Fig. 3b). Since the pressure near the upper wall is greater than near the bottom, a transversal pressure gradient arises, which makes the gas move from top to bottom. The resultant gas flow, after its collision with the bottom wall, rolls up into a vortex (see Fig. 2b). As the reflected shock wave is shifted to the left, the vortex is extended, and its transversal size increases until the vortex fills up the whole channel section. The front of the shock wave becomes straight when the latter comes out from the particle cloud, and then the shock wave is separated from the vortex. The particles entering the vortex region are first decelerated and then lifted. Further, the flow remains qualitatively unchanged, and the particles occupy the greater part of the channel cross section (Fig. 4). The gas velocity in the vortex reaches 150 m/sec. As a result, the Magnus force $\boldsymbol{F}_{\mathrm{M}}$ and aerodynamic drag $(\boldsymbol{v}_1 - \boldsymbol{v}_2)/\tau$ are rather large, which ensures lifting of particles 200 μm in diameter.

To evaluate the Magnus force, a calculation with the above parameters was performed, but the Magnus force in the corresponding equations of system (1) was taken equal to zero. The calculated velocity fields $\boldsymbol{v}_1$ and isolines of the volume concentration of particles are shown in Fig. 5. A comparison with Fig. 4 shows that the velocity field is changed weakly, and the particles are lifted slower than in the case of the Magnus force taken into account. However, if we compare the number of particles $N_2 \approx \int m_2(x, y)\, dx$ lifted to the height $y_2 = 1$ cm quantitatively, we see that this difference is not too great. Thus, the contributions of the Magnus force and aerodynamic drag to particle lifting behind the reflected shock wave are commensurable.

Thus, results of numerical simulation of dust lifting behind a shock wave reflected from the end-face wall of the channel are presented. A vortex flow behind the reflected shock wave is found. It is shown that particle lifting occurs in the vortex under the effect of the Magnus force and aerodynamic drag. The values of the Magnus force and aerodynamic drag in the vortex are comparable.

REFERENCES

1. A. A. Borisov, A. V. Lyubimov, S. M. Kogarko, and V. P. Kozenko, "Instability of grainy media with a sliding shock wave and detonation waves," *Fiz. Goreniya Vzryva*, **3**, No. 1, 149–151 (1967).
2. K. Bracht and W. Merzkich, "The erosion of dust by a shock wave in air: initial studies with laminar flow," *Int. J. Multiphase Flow*, **4**, No. 1, 89–95 (1978).
3. B. Fletcher, "The interaction of a shock with a dust deposit," *J. Phys. D. Appl. Phys.*, **9**, 197–202 (1976).

4. A. L. Kuhll, K. Chien, R. E. Ferguson, et al., "Simulation of a turbulent dusty boundary layer behind shock," in: *Current Topics in Shock Waves*, Proc. of the 17th Int. Symp. on Shock Waves and Shock Tubes, S. l., 762–769 (1990).
5. V. M. Boiko and A. N. Papyrin, "Dynamics of gas-suspension formation behind the shock wave sliding along the surface of a grainy media," *Fiz. Goreniya Vzryva*, **23**, No. 2, 122–126 (1987).
6. V. M. Boiko, "Laser diagnostics of microprocesses in interaction of shock waves and liquid/solid particles," Doctoral Dissertation in Phys.-Math. Sci., Novosibirsk (1995).
7. S. P. Kiselev and V. P. Kiselev, "Ignition of pulverized coal particles in shock waves," *Prikl. Mekh. Tekh. Fiz.*, **36**, No. 3, 31–37 (1995).
8. S. P. Kiselev, E. V. Vorozhtsov, and V. M. Fomin, *Foundations of Fluid Mechanics with Applications: Problem Solving Using Mathematica*," Birkhauser, Boston–Basel–Berlin (1999).
9. V. P. Kiselev, S. P. Kiselev, and V. M. Fomin, "Interaction of a shock wave with a cloud of particles of finite dimensions," *Prikl. Mekh. Tekh. Fiz.*, **35**, No. 2, 26–37 (1994).
10. M. A. Gol'dshtik and B. N. Kozlov, "Elementary theory of concentrated dispersed systems," *Prikl. Mekh. Tekh. Fiz.*, No. 4, 67–77 (1973).
11. M. A. Gol'dshtik and V. N. Sorokin, "Particle motion in a vortex chamber," *Prikl. Mekh. Tekh. Fiz.*, No. 6, 149–152 (1968).